Thermoelectric power factor of Ge1-Sn thin films

A. Portavoce, H. Khelidj, N. Oueldna, S. Amhil, M. Bertoglio, D. Mangelinck, L. Essaleh, K. Hoummada

Thermoelectric power factor of $Ge_{1-x}Sn_x$ thin films

A. Portavoce[1*], H. Kelidge[1,2], N. Oueldna[1,3], S. Amhil[4], M. Bertoglio[1], D. Mangelinck[1], L. Essaleh[4], and K. Hoummada[1]

[1]*IM2NP, CNRS/Aix-Marseille University, Faculté des Sciences de Saint-Jérôme case 142, 13397 Marseille, France*
[2]*L3M, Ecole Nationale Supérieure des Mines et de la Métallurgie, Annaba, Algeria*
[3]*LASMAR, University of Moulay Ismail, Faculté des Sciences, 11201 Meknes, Morocco*
[4]*LMCN, Cadi-Ayyad University, Faculty of Sciences and Technology, Department of Applied Physics, Marrakech, Morocco*

ABSTRACT

The Seebeck coefficients (α) and the power factors of 100 nm-thick $Ge_{1-x}Sn_x$ films grown by magnetron sputtering were studied versus Sn composition ($0.09 \leq x \leq 0.15$) in the 220–330 K temperature range. The films present particularly high Seebeck coefficients at room temperature. However, their power factors are too low for room temperature thermoelectric applications due to low electrical conductivity (σ). Nevertheless, owing the possibility of modifying both α and σ by adjusting x, combined with conventional doping capabilities, the IV-IV $Ge_{1-x}Sn_x$ semiconductor is shown to be potentially interesting for complementary-metal-oxide-semiconductor-compatible thermoelectric applications.

Keywords: $Ge_{1-x}Sn_x$, Thin films, Seebeck coefficient, Thermoelectricity

[*]Corresponding author: alain.portavoce@im2np.fr

Thermoelectric technology can be used for heat-to-electricity conversion [1]. In this case, thermoelectric devices exploit a temperature (T) gradient to produce electricity. Their performance is mainly depending on inherent material properties, such as Seebeck coefficient (α), electrical conductivity (σ), and thermal conductivity (κ) [1]. High-performance thermoelectric devices should use high-performance thermoelectric materials exhibiting a high power factor $PF = \alpha^2\sigma$ and the highest possible figure of merit $ZT = \alpha^2\sigma T/\kappa$. With the development of mobile microelectronic and communication devices, the technologies of energy conversion face new challenges, as they are expected to offer energy harvesting solutions that can be integrated to microelectronic circuits [2]. The goal of integrated energy harvesting devices is to use surrounding energy sources (thermal, mechanical, electromagnetic waves…) to produce electricity that can be used by the mobile device during operation, allowing its autonomy to be increased. This electricity production can be used either to partially charge the device battery (or an integrated supercapacitor), or to execute some operations without soliciting the battery. Thermoelectric devices should be particularly convenient for this type of application, since temperature gradients are generally present in microelectronic setups. Furthermore, the required energy supply stays modest, as it does not need to entirely power the device, and mobile devices use generally low-consumption microelectronic circuits. Additionally, thermoelectric modules are solid-state and can be miniaturized. However, microelectronic applications require specific technological restrictions: energy harvesting must be performed at temperatures close to room temperature (RT), and in order to be integrated in microelectronic technology, materials as well as their elaboration processes must be compatible with the complementary metal-oxide-semiconductor (CMOS) technology [2]. Moreover, the integrated device should be based on thin films (micro- or nanostructure), and if possible, made of abundant and nontoxic materials. Accordingly, current thermoelectric materials exhibiting the best thermoelectric

properties at RT cannot be used for microelectronic applications. They are not compatible with the CMOS technology, and use toxic or scarce elements, such as $Bi_{2-x}Sb_xTe_3$ (*p*-type) and $Bi_2Te_{3-x}Se_x$ (*n*-type) compounds, for example [3-4]. Semiconductors are materials of particular interest for thermoelectric applications, especially due to their doping possibility. The same semiconductor can be either *p*- or *n*-type controlling dopant nature (control of the carrier type: electrons or holes), and the semiconductor Fermi level as well as the carrier concentration can be adjusted controlling the dopant concentration, allowing for material *ZT* engineering [5-6].

Ge(Sn) is a CMOS-compatible IV-IV semiconductor, currently investigated for CMOS optoelectronic applications as well as for Si photonics [7-11]. The $Ge_{1-x}Sn_x$ alloy forms a Ge-Sn binary random solution exhibiting the cubic diamond structure with a lattice parameter a_{GeSn} larger than Ge, following the corrected-Vegard law

$$a_{GeSn} = (1-x)a_{Ge} + xa_{Sn} + bx(1-x) \quad (1)$$

With a_{Ge} = 0.565 nm et a_{Sn} = 0.649 nm, the Ge and Sn lattice parameters in the diamond structure, respectively, and b = 0.0041 nm the bowing coefficient [12-14]. Sn maximum solubility in Ge is only 1.1 at% at 673 K [15].

Though, meta-stable Sn-rich $Ge_{1-x}Sn_x$ thin films can be elaborated [16]. Interestingly for thermoelectric applications, $Ge_{1-x}Sn_x$ alloys can possess higher carrier mobility [17-19] than Ge and lower thermal conductivities [20-21]. Furthermore, Sn composition variations are known to involve serious modifications of the $Ge_{1-x}Sn_x$ alloy electronic band structure, the semiconductor electronic band gap being indirect for $x \leq 0.1$ and being direct for $x \geq 0.1$ [22-

24]. Consequently, the $Ge_{1-x}Sn_x$ Seebeck coefficient is expected to be significantly dependent on the alloy Sn composition, allowing for significant degree of freedom for *ZT* engineering. $Ge_{1-x}Sn_x$ films are usually elaborated by molecular beam epitaxy or chemical vapour deposition [13-14,16-19]. However, magnetron sputtering seems more appropriate for thermoelectric applications [12, 25], since it involves a significantly lower production cost, while being CMOS-compatible. This work reports the investigation of the Seebeck coefficient and power factor variations of 100-nm-thick $Ge_{1-x}Sn_x$ films with Sn composition ($0.09 \leq x \leq 0.15$) in the temperature range $220 \leq T \leq 330$ K, for CMOS-compatible RT energy harvesting.

100 nm-thick $Ge_{1-x}Sn_x$ films were deposited in a commercial magnetron sputtering system (base pressure of 10^{-8} Torr) at T = 673 K on 1.5 × 2.5 cm^2 glass substrates. The substrates were subsequently cleaned 10 min in acetone and alcohol baths in an ultrasonic cleaner, and kept 30 min at 423 K in a baking furnace, before to be loaded in the sputtering chamber. Commercial 99.999% Ge-pure and 99.99% Sn-pure targets were co-sputtered using different sputtering powers for Sn in order to get different Sn compositions from x = 0.0 to x = 0.15. Ge and Sn deposition fluxes were calibrated thanks to ex-situ thickness measurements using X-ray reflectivity. $Ge_{1-x}Sn_x$ film concentrations were determined using X-ray diffraction (XRD), and checked using Rutherford back scattering and atom probe tomography measurements. The structure of the films was investigated using XRD in the Bragg-Brentano (θ-2θ) geometry using a Cu K_α source ($\lambda_{K\alpha}$ = 0.154 nm). The surface state of the films was checked by atom force microscopy (AFM). The film electrical conductivities were measured versus temperature by impedance spectroscopy [26] using an impedance analyzer (HP 4284 A) operated between 20 Hz and 1 MHz, using an alternative signal of amplitude 100 mV. Contacts on the samples were achieved using a silver conductive paste. The temperature variations were controlled using a programmable Thermolyne heater, or using a liquid

nitrogen cryostat for the low temperatures. The Seebeck coefficients of the films were measured using a home-made setup [27].

Figure 1 shows AFM images of the glass substrate before deposition (fig. 1a) as well as of three $Ge_{1-x}Sn_x$ films with x = 0.09, 0.13, and 0.15 (figs. 1b–1d). The surface roughness of the three films is significantly smaller than their thickness (< 5%). It is smaller than the glass substrate roughness (5.13 nm), and is smaller for higher Sn concentrations (4.56, 2.75, and 2.31 nm for x = 0.09, 0.13, and 0.15, respectively). Figure 2a shows the X-ray diffractograms measured in the Bragg-Brentano geometry on four samples with x = 0.0, 0.09, 0.13, and 0.15. The films are polycrystalline and exhibit the same texture along the normal of the surface: the same four diffraction peaks are observed for each sample, corresponding (from left to right) to the (111), (220), and (311) atomic planes of the diamond structure. Pure-Sn diffraction peaks are not detected. As expected, the shift of $Ge_{1-x}Sn_x$ diffraction peaks towards the lower angles (Fig. 2b) corresponds to x = 0.09, 0.13, and 0.15 according to eq. 1. Figure 3a presents the electrical conductivities measured on the three $Ge_{1-x}Sn_x$ films versus temperature, in the 220-330 K temperature range. σ increases with temperature, as expected for semiconductor layers. Furthermore, σ increases also with x, the conductivity of the $Ge_{1-x}Sn_x$ films being higher than the conductivity of intrinsic Ge. For example, σ = 0.029, 3.08, and 9.05 Ω^{-1} cm^{-1} at 300 K for x = 0.09, 0.13, and 0.15, respectively, while $\sigma \sim 0.02$ Ω^{-1} cm^{-1} for undoped Ge at the same temperature [28]. One can note that the conductivity of the $Ge_{91}Sn_{0.09}$ film is significantly lower (~ two orders of magnitude) than that of the two other $Ge_{0.87}Sn_{0.13}$ and $Ge_{0.86}Sn_{0.15}$ films. This difference may be related to the significant electronic band structure difference between $Ge_{1-x}Sn_x$ alloys of Sn compositions below (indirect band gap) and above (direct band gap) x = 0.1 [22-23]. The Seebeck coefficients of the $Ge_{1-x}Sn_x$ films measured in the same temperature range are shown in Figure 3b. α is positive for the three films, corresponding to *p*-type semiconductors. The Seebeck coefficients

of the $Ge_{1-x}Sn_x$ films is found to be significantly high around RT, with α = 120, 300, and 248 µV K^{-1} at 300 K for x = 0.09, 0.13, and 0.15, respectively. Sn composition variations have a strong impact on the Seebeck coefficient. α variations versus temperature are different in each film. Furthermore, α variations are not proportional to x, since at given temperature $\alpha(x = 0.09) \leq \alpha(x = 0.15) \leq \alpha(x = 0.13)$. The Seebeck coefficient difference between the films is important despite relatively low composition variations, as a difference of about 100 µV K^{-1} separates $\alpha(x = 0.09)$ from $\alpha(x = 0.15)$, as well as $\alpha(x = 0.15)$ from $\alpha(x = 0.13)$. These observations should be related to major differences in the electronic density-of-state of the three alloys, and show that alloying Ge with Sn significantly modifies the average energy (E), the concentration (n), the effective mass (m^*), or the scattering coefficient (γ) of the charge carriers (of charge q) of the alloy in the Fermi level vicinity (E_F), since α is known to be dependent on these parameters in degenerated semiconductors (eq. 2) [3, 29].

$$\alpha = \frac{E-E_F}{q\Delta T} \propto \frac{m^*T}{q}\left(\frac{\pi}{3n}\right)^{\frac{2}{3}}\left(\frac{3}{2}+\gamma\right) \qquad (2)$$

Equation 2 shows that the increase of α through the modification of any of these parameters results in a decrease of the electronic conductivity. Sn composition is shown to be an important parameter allowing for the simultaneous modification of α and σ. As expected, the increase of α can be associated to a decrease of σ (eq. 2): when x decreases from 0.15 to 0.13, α increases from 248 to 300 µV K^{-1} and σ decreases from 9.05 to 3.08 Ω^{-1} cm^{-1} at T = 300 K. However, x modification can also remarkably lead to the concomitant increase of α and σ, when x increases from 0.09 to 0.13 or 0.15 (Fig. 3), for example. Figure 4 presents the PF variations of the $Ge_{1-x}Sn_x$ films versus temperature. The PF increases with x despite that $\alpha(x = 0.15) \leq \alpha(x = 0.13)$. Due to the large difference of electrical conductivity, the PF of the

$Ge_{91}Sn_{0.09}$ film (4.2×10^{-4} µW cm^{-1} K^{-2} at 300 K) is a lot lower than that of the two other $Ge_{0.87}Sn_{0.13}$ (0.44 µW cm^{-1} K^{-2} at 300 K) and $Ge_{0.86}Sn_{0.15}$ (0.56 µW cm^{-1} K^{-2} at 300 K) films. Despite significantly high Seebeck coefficients, the *PF* of the films is two orders of magnitude smaller (for x = 0.13 and 0.15) than that of current best materials for RT thermoelectric applications, such as $Bi_{2-x}Sb_xTe_3$ [30], SnSe [31], $SnS_{091}Se_{0.09}$ [32] or $Mg_2Sn_{0.75}Ge_{0.25}$ [33]. The $Ge_{1-x}Sn_x$ *PF* is actually impaired by the low electrical conductivity of the films. For example, for x = 0.13 at 300 K α = 300 µV K^{-1} but σ = 3.08 Ω^{-1} cm^{-1} leading to *PF* = 0.44 µW cm^{-1} K^{-2}. However, former works shown that Ge doping with Sn concentrations of about 10^{19} at cm^{-3} ($x = 1 \times 10^{-3}$) is of *p*-type and leads to $\sigma \sim 1$ Ω^{-1} cm^{-1} with $n \sim 2.2 \times 10^{16}$ cm^{-3} [34]. One can note that the hole concentration is in this case three orders of magnitude smaller than the concentration of Sn, and the conductivity of these low-Sn-concentrated layers is of the same magnitude as that of our high-concentrated films. This is usually explained considering that the hole concentration occurs from charged point defects [17-18]. Thus, despite the significant difference of Sn concentration, our films are also expected to be weakly doped [19]. Consequently, doping the $Ge_{1-x}Sn_x$ films with regular dopants such as B can be an interesting way to significantly increase the electrical conductivity of $Ge_{1-x}Sn_x$ films, likely boosting their power factors. Indeed, $Ge_{1-x}Sn_x$ *p*-type and *n*-type doping three orders of magnitude higher (n = 1 to 5 × 10^{19} cm^{-3}) have been demonstrated using As, P, and B [35].

In conclusion, the power factor of 100 nm-thick $Ge_{1-x}Sn_x$ films with $0.09 \leq x \leq 0.15$ has been determined aiming for RT CMOS-compatible thermoelectric applications. The $Ge_{1-x}Sn_x$ films are *p*-type and possess Seebeck coefficients particularly high at RT. As expected, variations of Sn composition result to significant modifications of the Seebeck coefficient without proportional relation with x. The low electrical conductivity of the layers

leads to power factors too low for RT applications. Though, the Sn composition is shown to be an efficient parameter for modifying both α and σ, sometimes allowing for the concomitant increase of these two factors. Thus, the possibility of adjusting the alloy Sn composition combined with structural and doping modification capabilities offer significant degrees of freedom for $Ge_{1-x}Sn_x$ *PF* and *ZT* engineering. Therefore, $Ge_{1-x}Sn_x$ is a CMOS-compatible semiconductor showing interesting potential for thermoelectric applications. In particular, the electrical conductivity of $Ge_{1-x}Sn_x$ films being potentially increased by three orders of magnitude by conventional doping, $Ge_{1-x}Sn_x$ films may still be interesting for RT thermoelectric applications.

REFERENCES

[1] A. Shakouri, Annu. Rev. Mater. Res 41, 399 (2011).

[2] A.P. Perez-Marin, A.F. Lopeandia, L. Abad, P. Ferrando-Villaba, G. Garcia, A.M. Loopez, F.X. Muñoz-Pascual, J. Rodriguez-Viejo, Nano Energy 4, 73 (2014).

[3] Y.C. Dou, X.Y. Qin, D. Li, L.L. Li, T.H. Zou, and Q.Q. Wang, J. Appl. Phys. 114, 044906 (2013).

[4] E. Pozega, S. Ivanov, Z. Stevic, L. Karanovic, R. Tomanec, L. Gomidzelovic, A. Kostov, Trans. Nonferrous Met. Soc. China 25, 3279 (2015).

[5] G. Tan, L.-D. Zhao, and M.G. Kanatzidis, Chem. Rev. 116, 12123 (2016).

[6] J. He and T.M. Tritt, Science 357, 1369 (2017).

[7] Z. Fang, Q.Y. Chen, and C.Z. Zhao, Optics & Laser Echnno. 46, 103 (2013).

[8] K.P. Homewood and M.A. Lourenço, Nature Photonics 9, 78 (2015).

[9] Z. Zhou, B. Yin, and J. Michel, Light: Sci. Appl. 4, e358 (2015).

[10] D. Thomson, A. Zilkie, J.E. Bowers, T. Komljenovic, G.T. Reed, L. Vivien, D. Marris-Morini, E. Cassan, L. Virot, J.-M. Fédéli, J.-M. Hartmann, J.H. Schmid, D.-X. Xu, F. Boeuf, P. O'Brien, G.Z. Mashanovich, and M. Nedeljkovic, J. Opt. 18, 073003 (2016)

[11] W. Du and S.-Q. Yu, Mid-infrared Optoelectronics 12, 493 (2020), doi: https://doi.org/10.1016/B978-0-08-102709-7.00012-7

[12] H. Mahmodi, M.R. Hashim, U. Hashim, Superlattices and Microstructures 98, 235 (2016).

[13] C. Xu, C.L. Senaratne, R.J. Culbertson, J. Kouvetakis, and J. Menéndez, J. Appl. Phys. 122, 125702 (2017).

[14] Y.-H Kil, S. Kang, T.S. Jeong, K.-H. Shim, D.-J. Kim, Y.-D. Choi, M.J. Kim, T.S. Kim, Journal of the Korean Physical Society 72, 1063 (2018).

[15] A. Gokhale and G. J. Abbaschian, Binary Alloy Phase Diagrams, 2nd ed. (ASM International, 1990), Vol. 2, p. 1964.

[16] M. Oehme, K. Kostecki, M. Schmid, F. Oliveira, E. Kasper, J. Schulze, Thin Solid Films 557, 169 (2014).

[17] W. Takeuchi, N. Taoka, M. Kurosawa, M. Sakashita, O. Nakatsuka, and S. Zaima, Appl. Phys. Lett. 107, 022103 (2015).

[18] T. Sadoh, Y. Kai, R. Matsumura, K. Moto, and M. Miyao, Appl. Phys. Lett. 109, 232106 (2016).

[19] K. Moto, R. Yoshimine, T. Suemasu, and K. Toko, Sci. Rep. 8, 14832 (2018).

[20] N. Uchida, T. Maeda, R.R. Lieten, S. Okajima, Y. Ohishi, R. Takase, M. Ishimaru, and J.-P. Locquet, Appl. Phys. Lett. 107, 232105 (2015).

[21] S.N. Khatami and Z. Aksamija, Phys. Rev. Appl. 6, 014015 (2016).

[22] H. Pérez Ladrón de Guevara, A.G. Rodríguez, H. Navarro-Contreras, and M.A. Vidal, Appl. Phys. Lett. 84, 4532 (2004).

[23] S. Wirths, R. Geiger, N. von den Driesch, G. Mussler, T. Stoica, S. Mantl, Z. Ikonic, M. Luysberg, S. Chiussi, J.M. Hartmann, H. Sigg, J. Faist, D. Buca, and D. Grützmacher, Nature Photonics 9 , 88 (2015).

[24] T.D. Eales, I.P. Marko, S. Schulz, E. O'Halloran, S. Ghetmiri, W. Du, Y. Zhou, S.-Q. Yu, J. Margetis, J. Tolle, E.P. O'Reilly, and S.J. Sweeney, Sci. Rep. 9, 14077 (2019).

[25] J. Zheng, L. Li, T. Zhou, Y. Zuo, C. Li, B. Cheng, and Q. Wang, ECS Sol. State Lett. 3, P111 (2014).

[26] A. Kaushal, S.M. Olhero, Budhendra Singh, Duncan P. Fagg, Igor Bdikin, J.M.F. Ferreira, Ceramics International 40, 10593 (2014).

[27] N. Oueldna, A. Portavoce, M. Bertoglio, M. Descoins, A. Kammouni, K. Hoummada, Materials Letters 266, 127460 (2020).

[28] D.B. Cuttris, Bell Syst. Techn. J. 40, 509 (1961).

[29] V. Vargiamidis, M. Thesberg, and N. Neophytou, J. Appl. Phys. 126, 055107 (2019).

[30] B. Poudel, Q. Hao, Y. Ma, Y. Lan, A. Minnich, B. Yu, X. Yan, D. Wang, A. Muto, D. Vashaee, X. Chen, J. Liu, M.S. Dresselhaus, G. Chen, Z. Ren, Science 320, 634 (2008).

[31] L.-D. Zhao, G. Tan, S. Hao, J. He, Y. Pei, H. Chi, H. Wang, S. Gong, H. Xu, V.P. Dravid, C. Uher, G.J. Snyder, C. Wolverton, and M.G. Kanatzidis, Science 351, 141 (2016).

[32] W. He, D. Wang, H. Wu, Y. Xiao, Y. Zhang, D. He, Y. Feng, Y.-J. Hao, J.-F. Dong, R. Chetty, L. Hao, D. Chen, J. Qin, Q. Yang, X. Li, J.-M. Song, Y. Zhu, W. Xu, C. Niu, µX. Li, G. Wang, C. Liu, M. Ohta, S.J. Pennycook, J. He, J.-F. Li, and L.-D. Zhao, Science 365, 1418 (2019).

[33] W. Liu, H.S. Kim, S. Chen, Q. Jie, B. Lv, M. Yao, Z. Ren, C.P. Opeil, S. Wilson, C.-W. Chu, and Z. Ren, Proc. Nat. Ac. Sci. 112, 3269 (2015).

[34] R. Roucka, R. Beeler, J. Mathews, M.-Y. Ryu, Y.K. Yeo, J. Menéndez, and J. Kouvetakis, J. Appl. Phys. 109, 103115 (2011).

[35] J. Xie, J. Tolle, V.R. D'Costa, C. Weng, A.V.G. Chizmeshya, J. Menendez, J. Kouvetakis, Solid-State Electronics 53, 816 (2009).

CAPTIONS

FIG. 1. AFM images obtained on the glass substrate surface before growth (a) as well as after the growth of a 100 nm-thick $Ge_{1-x}Sn_x$ film with x = 0.09 (b), 0.13 (c), and 0.15 (d).

FIG. 2. X-ray diffractograms measured on $Ge_{1-x}Sn_x$ films with x = 0.0, 0.09, 0.13, and 0.15.

FIG. 3. Electrical conductivity (a) and Seebeck coefficient (b) measured versus temperature on three different 100 nm-thick $Ge_{1-x}Sn_x$ films with x = 0.09, 0.13, and 0.15.

FIG. 4. $Ge_{1-x}Sn_x$ film power factors versus temperature determined from the electrical conductivities and the Seebeck coefficients presented in fig. 3.

Figure 1

A. Portavoce et al.

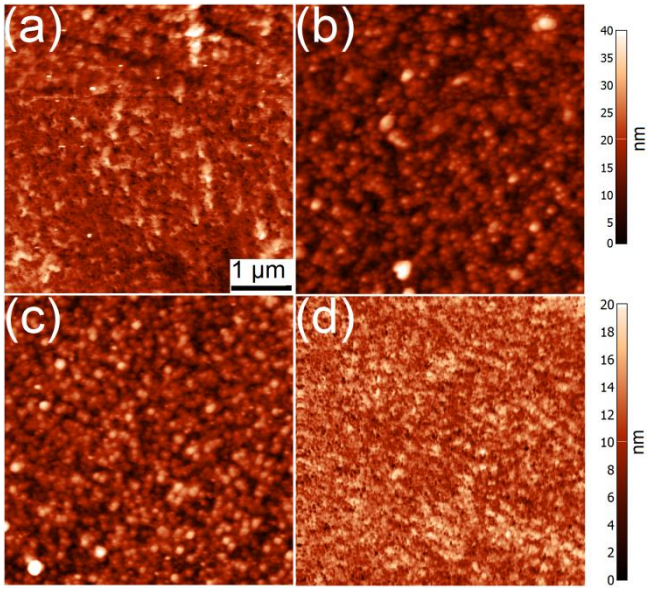

Figure 2

A. Portavoce et al.

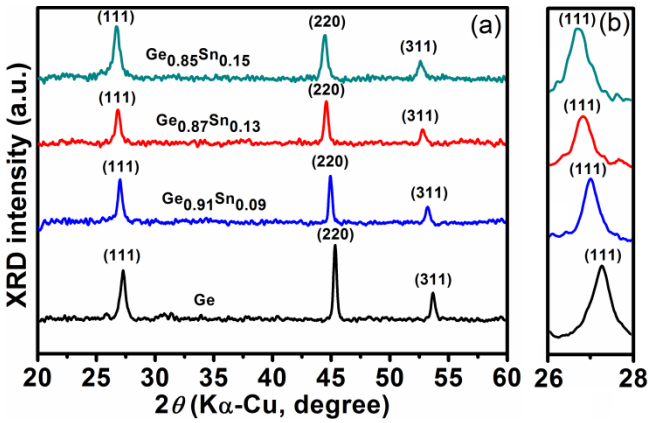

Figure 3

A. Portavoce et al.

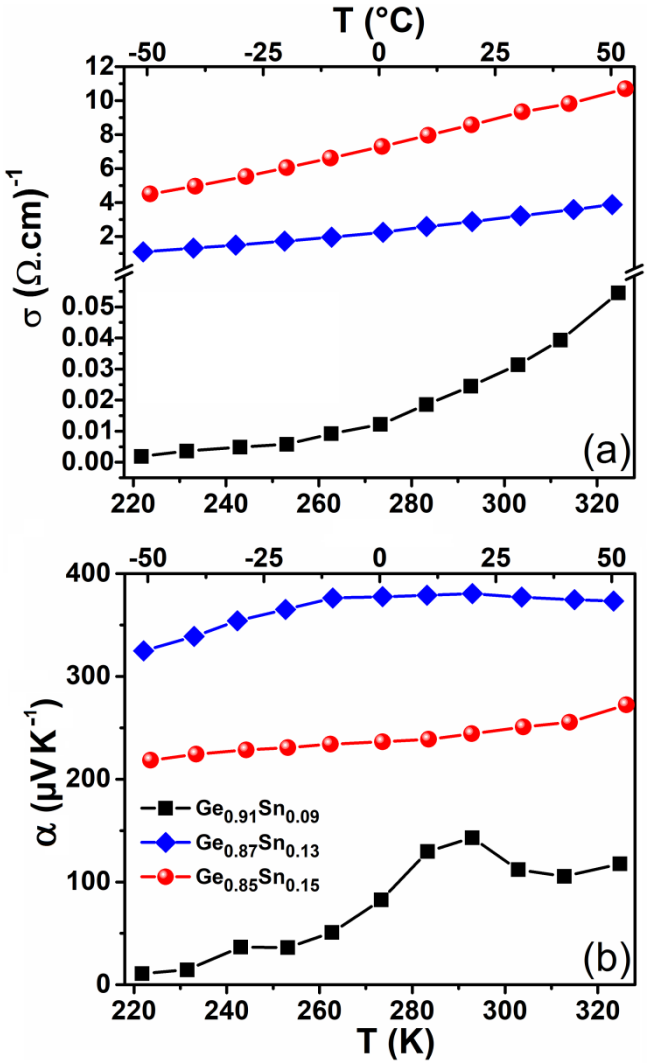

Figure 4

A. Portavoce et al.